On the sound fields of infinitely long strips

Tim Mellow
Nokia UK Ltd., Nokia House, Summit Avenue, Farnborough, Hants GU14 0NG, United Kingdom

Leo Kärkkäinen
Nokia Research Center, Itämerenkatu 11-13, 00180 Helsinki, Finland

(Received 10 September 2010; revised 9 May 2011; accepted 11 May 2011)

Exact solutions are derived for sound radiation from four kinds of infinitely-long strips: namely a rigid strip in a baffle of finite width, a resilient strip in free space, and a resilient or rigid strip in an infinite baffle. In one limit, the strip in a finite baffle becomes a rigid strip in free space and in the other, a line source in a finite baffle. Here "rigid" means that the surface velocity is uniform, whereas "resilient" means that the surface pressure is uniform, and the strip is assumed to have zero mass or stiffness, as if a force were driving the acoustic medium directly. According to the Babinet–Bouwkamp principle, radiation from a resilient strip in an infinite baffle is equivalent to diffraction of a plane wave through a slit in the same. Plots are shown for the radiation impedances, far-field directivity patterns, and on-axis pressure responses of the four kinds of strip. A simple relationship between the radiation admittance of the rigid strip in an infinite baffle and the resilient strip in free space is presented. The two-dimensional rectangular wave functions developed in this paper can be applied to related problems.
[DOI: 10.1121/1.3596474]

PACS number(s): 43.38.Ar, 43.20.Rz, 43.20.Bi, 43.20.El [TDM] Pages: 153–167

I. INTRODUCTION

The acoustical impedance of the air load on a transducer diaphragm of low mass and high aspect ratio has a significant influence upon its motion and is therefore an important factor in its design. Practical examples of such transducers are ribbon loudspeakers and microphones or loudspeakers comprising arrays of electrostatic[1] or planar magnetic strip radiators in configurations designed to give wide horizontal sound dispersion but narrow vertical dispersion. Previous studies[2–4] have focused on the rigid strip in an infinite baffle because it yields a closed-form solution, but arguably a more realistic model is that of a strip in a baffle of finite width or free space as analyzed here.

The related problems of diffraction by a slit in a rigid screen and scattering by a rigid strip, where the former is equivalent to radiation from a resilient strip in an infinite baffle and the latter a rigid strip in free space, were computed by Morse and Rubinstein[5] using Mathieu functions, which are greatly complicated by the fact that a whole sequence of elliptical harmonics has to be computed at each frequency step. In this paper, the problems are simplified by using the boundary integral method with an integral Green's function that represents an inverse Fourier transform of the propagated source spectra. This leads to analytical solutions in the form of simultaneous equations.

Although Babinet[6] first postulated a relationship between the scattered field of a plane wave incident upon an aperture in a planar screen and the field scattered from the complementary shape removed in order to form the aperture, it was Bouwkamp[7] who formalized this mathematically. The scattered fields are only identical in two cases: When the screen is perfectly rigid but the complementary shape is perfectly resilient and *vice versa*. Hence the term Babinet–Bouwkamp principle would appear to be an apt nomenclature for this description. In this paper, the resilient strip in an infinite baffle provides the scattered field for the first case and the rigid strip in free space the second.

One configuration not considered in this paper is that of a resilient strip in a finite baffle. If the baffle were rigid, the problem would be greatly complicated by the fact that boundary conditions across the strip and baffle would be a mixture of pressure and velocity, rendering the methods used in the rest of the paper inapplicable. Similar methods could in theory be used to analyze a monopole resilient strip in a resilient (*i.e.* pressure release) baffle, but this would bear little resemblance to any practical application.

Although the approach used here has similarities with that previously used to analyze rigid[8,9] and resilient disks in baffles[10] and free space,[11] the integral Green's function in cylindrical coordinates must first be recast into one in rectangular coordinates. As can be seen from Eq. (A20) in the Appendix, the problem is complicated by the fact that the half-integer order expansions for the disk are replaced integer order expansions for the strip which contain logarithmic and digamma functions. In Sec. II of this paper, the radiation impedance and far-field pressure response of a rigid strip in a finite baffle (or free space) is derived. In Sec. III, the radiation impedance of a resilient strip in free space is also given. In Sec. IV, the radiation impedance and far-field pressure response of a resilient strip in an infinite baffle is derived. As an example of the utility of the integral Green's function, the radiation impedance of a rigid strip in an infinite baffle is reproduced in just a few steps in Sec. V.

II. RIGID STRIP IN A FINITE BAFFLE

A. Boundary conditions

The strip of width $2a$ shown in Fig. 1 is mounted in a finite baffle of width $2d$ in the xy plane with its line of symmetry on the y axis and oscillates in the z direction with a harmonically time dependent velocity $\tilde{u}_0$, thus radiating from both sides into a homogeneous loss-free medium. The pressure field on one side of the xy plane is the symmetrical "negative" of that on the other, so that

$$\tilde{p}(x,z) = -\tilde{p}(x,-z). \tag{1}$$

Consequently, there is a Dirichlet boundary condition in the plane of the strip where these equal and opposite fields meet

$$\tilde{p}(x,0) = 0, \quad -\infty \le x < -d, \quad d < x \le \infty, \tag{2}$$

which is satisfied automatically. On the front and rear surfaces of the baffle, there is a Neumann boundary condition

$$\frac{\partial}{\partial z}\tilde{p}(x,z)|_{z=0\pm} = 0, \quad -d \ge x > -a, \quad a < x \le d. \tag{3}$$

Also, on the front and rear surfaces of the strip, there is the coupling condition

$$\frac{\partial}{\partial z}\tilde{p}(x,z)|_{z=0} = -jk\rho_0 c\tilde{u}_0, \quad -a \le x \le a, \tag{4}$$

where k is the wave number given by $k = \omega/c = 2\pi/\lambda$, ω is the angular frequency of excitation, ρ_0 is the density of the surrounding medium, c is the speed of sound in that medium, and λ is the wavelength. On the front and rear surfaces of the strip and baffle, the unknown pressures are $\tilde{p}_+$ and $\tilde{p}_-$, respectively, for which a suitable trial function must be devised that satisfies the boundary condition of zero pressure at the edge. Here we adapt the trial function previously used for a disk in a circular baffle[8]:

$$\tilde{p}_+(x_0,0) = -\tilde{p}_-(x_0,0) = \rho c\tilde{u}_0 \sum_{n=0}^{\infty} A_n \left(1 - \frac{x_0^2}{d^2}\right)^{n+\frac{1}{2}}, \quad -d \le x_0 \le d. \tag{5}$$

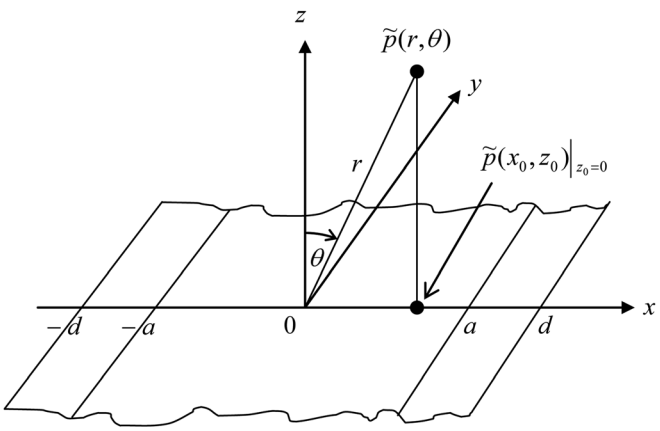

FIG. 1. Geometry of the infinite strip of width $2a$ in a baffle of width $2d$.

where A_n are the as yet unknown power series coefficient that will be calculated by means of a set of simultaneous equations in matrix form.

B. Boundary integral

The nearfield pressure is given by the dipole Rayleigh integral or dipole part of the Kirchhoff–Helmholtz boundary integral taking into account the surface pressure on both faces of the piston

$$\tilde{p}(x,z) = -\int_{-d}^{d} (\tilde{p}_+(x_0,0) - \tilde{p}_-(x_0,0)) \times \frac{\partial}{\partial z_0} g(x,z|x_0,z_0)|_{z_0=0} dx_0. \tag{6}$$

The classical Green's function in three-dimensional rectangular coordinates is given by

$$g(x,y,z|x_0,y_0,z_0) = \frac{e^{-ikR}}{4\pi R}, \tag{7}$$

where $R = \sqrt{(x-x_0)^2 + (y-y_0)^2 + (z-z_0)^2}$. This gives the spatial distribution observed at a point (x, y, z) due to a point source at (x_0, y_0, z_0). Using the Fourier transform into the wave-number domain, Morse *et al.*,[12] showed how this can be converted into an integral Green's function in cylindrical coordinates, often known as the Lamb[13] or Sommerfeld[14] integral, which several authors have used in order to investigate planar circular radiators.[8,15,16] However, this method is not restricted to just cylindrical coordinates and from Morse *et al.*,[12] it is fairly straight forward to show that in three-dimensional rectangular coordinates the integral Green's function becomes

$$g(x,y,z|x_0,y_0,z_0) = -\frac{i}{8\pi^2}\int_{-\infty}^{\infty}\int_{-\infty}^{\infty} \frac{e^{-i\left(k_x(x-x_0)+k_y(y-y_0)+k_z(z-z_0)\right)}}{k_z} dk_x dk_y \tag{8}$$

where

$$k_z = \begin{cases} \sqrt{k^2 - k_x^2 - k_y^2}, & k_x^2 + k_y^2 \le k^2 \\ -i\sqrt{k_x^2 + k_y^2 - k^2}, & k_x^2 + k_y^2 > k^2 \end{cases}. \tag{9}$$

When using this Green's function, the integral of Eq. (6) becomes a surface integral representing a Fourier transform of the pressure distribution in the x_0y_0 plane into k-space. The wave-number spectra is then propagated in the z direction to the xy plane where the integrals of Eq. (8) represent the inverse Fourier transform. This is the basis of nearfield acoustical holography,[17,18] which takes advantage of the fact that Eq. (8) allows the pressure field on either side of the x_0y_0 plane to be computed even if there are sources present, unlike Eq. (7). For finding analytical solutions, Eq. (8) also offers distinct advantages, even though it may seem counter intuitive to introduce extra integrals. For instance, taking the normal gradient of Eq. (7) leads to diverging integrals and

the variables within the square roots are difficult to separate unless complicated moveable-origin coordinate systems are used.[19,20]

In this paper, only systems of infinite extent in the y direction are considered, so that the classical Green's function of Eq. (7) reduces to the following two-dimensional form[21]

$$g(x,z|x_0,z_0) = -\frac{i}{4}H_0^{(1)}(kR), \tag{10}$$

where $H_0^{(1)}$ is the zeroth-order Hankel function and $R = \sqrt{(x-x_0)^2 + (z-z_0)^2}$. Likewise, Eq. (8) reduces to its two-dimensional counterpart

$$g(x,z|x_0,z_0) = -\frac{i}{4\pi}\int_{-\infty}^{\infty} \frac{e^{-i(k_x(x-x_0)+k_z(z-z_0))}}{k_z}dk_x, \tag{11}$$

where

$$k_z = \begin{cases} \sqrt{k^2-k_x^2}, & k_x^2 \le k^2 \\ -i\sqrt{k_x^2-k^2}, & k_x^2 > k^2 \end{cases}. \tag{12}$$

C. Formulation of the coupled equation for a rigid strip

Inserting Eqs. (5) and (11) into Eq. (6) and integrating over x_0 gives

$$\tilde{p}(x,z) = -\frac{d\rho c\tilde{u}_0}{\sqrt{\pi}}\sum_{n=0}^{\infty} A_n 2^n \Gamma\left(n+\tfrac{3}{2}\right) \times \int_{-\infty}^{\infty} \frac{J_{n+1}(k_x d)}{(k_x d)^{n+1}} e^{-i(k_x x + k_z z)}dk_x, \tag{13}$$

where Γ is the gamma function, J_n is the nth-order Bessel function of the first kind and the following differential-integral solution has been applied[22]

$$\int_{-d}^{d}\left(1-\frac{x_0^2}{d^2}\right)^{n+\frac{1}{2}} e^{ik_x x_0}dx_0 = 2\int_0^d \cos k_x x_0 \left(1-\frac{x_0^2}{d^2}\right)^{n+\frac{1}{2}}dx_0 = \sqrt{\pi}d2^{n+1}\Gamma\left(n+\tfrac{3}{2}\right)\frac{J_{n+1}(k_x d)}{(k_x d)^{n+1}}. \tag{14}$$

At the surface of the strip and baffle, there is the coupling condition

$$\frac{\partial}{\partial z}\tilde{p}(x,z)|_{z=0} = -ik\rho c\tilde{u}_0\Phi(x), \tag{15}$$

where $\mathbf{\Phi}(x)$ is a dimensionless function of the surface velocity distribution. We will use different expressions for $\mathbf{\Phi}(x)$ when considering a strip in free space and a strip or line source in a baffle of finite width. This leads to the following coupled equation

$$\sum_{n=0}^{\infty} A_n I_n(x) = -\Phi(x), \tag{16}$$

which is to be solved for the power series coefficients A_n. Letting $k_x = kt$, the integral $I_n(x)$ can be split into two parts

$$I_n(x) = I_{nR}(x) - iI_{nI}(x), \tag{17}$$

where the real part is given by

$$I_{nR}(x) = \frac{2^{n+1}\Gamma\left(n+\frac{3}{2}\right)kd}{\sqrt{\pi}}\int_0^1 \cos kxt \frac{J_{n+1}(kdt)}{(kdt)^{n+1}}\sqrt{1-t^2}dt, \tag{18}$$

and the imaginary part is given by

$$I_{nI}(x) = \frac{2^{n+1}\Gamma\left(n+\frac{3}{2}\right)kd}{\sqrt{\pi}}\int_1^\infty \cos kxt \frac{J_{n+1}(kdt)}{(kdt)^{n+1}}\sqrt{t^2-1}dt. \tag{19}$$

It is shown in the appendix that the solutions to these integrals are

$$I_{nR}(x) = \frac{1}{2}\sum_{m=0}^{\infty}\sum_{r=0}^{\infty}\frac{(-1)^{m+r}\Gamma\left(n+\frac{3}{2}\right)\Gamma\left(m+r+\frac{1}{2}\right)}{(2m)!r!(n+r+1)!(m+r+1)!} \times \left(\frac{kd}{2}\right)^{2m+2r+1}\left(\frac{2x}{d}\right)^{2m}, \tag{20}$$

$$I_{nI}(x) = \frac{1}{2\pi}\sum_{m=0}^{\infty}\left\{\sum_{r=0}^{\infty}\frac{(-1)^{m+r}\Gamma\left(n+\frac{3}{2}\right)\Gamma\left(m+r+\frac{1}{2}\right)}{(2m)!r!(n+r+1)!(m+r+1)!} \times \left(\frac{kd}{2}\right)^{2m+2r+1} \times \left(2\ln\left(\frac{kd}{2}\right) + \psi\left(m+r+\tfrac{1}{2}\right) - \psi(m+r+2) - \psi(r+1) - \psi(n+r+2)\right) - \sum_{r=0}^{n}\frac{(-1)^m(n-r)!\Gamma\left(n+\frac{3}{2}\right)\Gamma\left(m+r-n-\frac{1}{2}\right)}{(2m)!r!(m+r-n)!} \times \left(\frac{kd}{2}\right)^{2m+2r-2n-1}\right\}\left(\frac{2x}{d}\right)^{2m} \tag{21}$$

D. Solution of the power series coefficients for a rigid strip in free space

Equations (20) and (21) are both expansions in $(2x/d)^{2m}$. Hence, in order to solve for the expansion coefficients, it is useful to express the strip and baffle velocity distribution $\Phi(x)$ as a function of $(2x/d)^{2m}$. In the case of a strip in free space where $d=a$, the surface velocity distribution is

$$\Phi(x)|_{d=a} = 1 = \sum_{m=0}^{\infty}\delta_{m0}\left(\frac{2x}{a}\right)^{2m}, 0 \le x \le a, \tag{22}$$

where δ_{m0} is the Kronecker δ function defined by

$$\delta_{m0} = \begin{cases} 1, & m=0 \\ 0, & m \ne 0 \end{cases}, \tag{23}$$

Inserting Eqs. (17), (20), (21), and (22) in Eq. (16) and equating the coefficients of $(2x/a)^{2m}$ yields the following $(N+1)\times(N+1)$ matrix equation

$$\mathbf{M}\cdot\mathbf{a}=\mathbf{b}\Rightarrow\mathbf{a}=\mathbf{M}^{-1}\cdot\mathbf{b}, \tag{24}$$

where the matrix $\mathbf{M}$ and vectors $\mathbf{a}$ and $\mathbf{b}$ are given by

$$\mathbf{M}(m+1,n+1) = {}_n\mathbf{A}_m(ka)-i_n\mathbf{K}_m(ka), \quad \begin{cases} m=0,1,\ldots,N \\ n=0,1,\ldots,N \end{cases}, \tag{25}$$

$$\mathbf{b}(m+1)=-\delta_{m0}, \quad m=0,1,\ldots,N, \tag{26}$$

$$\mathbf{a}(n+1)=A_n, \quad n=0,1,\ldots,N, \tag{27}$$

and the infinite power series limits have been truncated to order N. The two-dimensional rectangular dipole wave functions ${}_n\mathbf{A}_m$ and ${}_n\mathbf{K}_m$ are defined by

$${}_n\mathbf{A}_m(ka) = \frac{1}{2}\sum_{r=0}^{N}\frac{(-1)^{m+r}\Gamma\left(n+\frac{3}{2}\right)\Gamma\left(m+r+\frac{1}{2}\right)}{(2m)!r!(n+r+1)!(m+r+1)!}\left(\frac{ka}{2}\right)^{2m+2r+1}, \tag{28}$$

$$\begin{aligned}{}_n\mathbf{K}_m(ka) &= \frac{1}{2\pi}\sum_{r=0}^{N}\frac{(-1)^{m+r}\Gamma\left(n+\frac{3}{2}\right)\Gamma\left(m+r+\frac{1}{2}\right)}{(2m)!r!(n+r+1)!(m+r+1)!}\left(\frac{ka}{2}\right)^{2m+2r+1}\\ &\times\left(2\ln\left(\frac{ka}{2}\right)+\psi\left(m+r+\tfrac{1}{2}\right)-\psi(m+r+2)\right.\\ &\left.-\psi(r+1)-\psi(n+r+2)\right)-\frac{1}{2\pi}\sum_{r=0}^{n}\\ &\times\frac{(-1)^m(n-r)!\Gamma\left(n+\frac{3}{2}\right)\Gamma\left(m+r-n-\frac{1}{2}\right)}{(2m)!r!(m+r-n)!}\\ &\times\left(\frac{ka}{2}\right)^{2m+2r-2n-1}.\end{aligned} \tag{29}$$

A truncation limit of $N=2ka$ was used for the calculations in this paper. For larger values of N, no discernable difference could be seen in the plots.

E. Solution of the power series coefficients for a rigid strip in a finite baffle

For a finite baffle, where $a\neq d$, we can employ the following *least-mean-squares* (LMS) algorithm. From Eq. (16), let an error function be defined by

$$E(A_n)=\int_{-d}^{d}\left|\sum_{n=0}^{\infty}A_nI_n(x)+\Phi(x)\right|^2dx. \tag{30}$$

where

$$\Phi(x)=\begin{cases}0, & -d\le x<-a\\ 1, & -a\le x\le a\\ 0, & a<x\le d\end{cases} \tag{31}$$

In order to find the values of A_n that minimize the error, we take the derivative of E with respect to A_n and equate the result to zero

$$\frac{\partial}{\partial A_n}E(A_n)=2\int_{-d}^{d}I_m(x)\left(\sum_{n=0}^{\infty}A_nI_n(x)+\Phi(x)\right)dx=0, \tag{32}$$

which, after truncating the infinite series limit to order N, yields the following set of $N+1$ simultaneous equations

$$\sum_{n=0}^{N}A_n\int_{-d}^{d}I_m(x)I_n(x)dx = -\int_{-a}^{a}I_m(x)dx, \quad m=0,1,\ldots,N, \tag{33}$$

where

$$I_m(x)=\sum_{p=0}^{\infty}\left({}_m\mathbf{A}_p(kd)-i_m\mathbf{K}_p(kd)\right)\left(\frac{2x}{d}\right)^{2p}, \tag{34}$$

$$I_n(x)=\sum_{q=0}^{\infty}\left({}_n\mathbf{A}_q(kd)-i_n\mathbf{K}_q(kd)\right)\left(\frac{2x}{d}\right)^{2q}. \tag{35}$$

Integrating over x yields the following $N\times N$ matrix equation

$$\mathbf{M}\cdot\mathbf{a}=\mathbf{b}, \tag{36}$$

where the matrix $\mathbf{M}$ and vectors $\mathbf{a}$ and $\mathbf{b}$ are given by

$$\mathbf{M}(m+1,n+1)=\sum_{p=0}^{P}\sum_{q=0}^{Q}\frac{2^{2q}\left({}_m\mathbf{A}_p(kd)-i_m\mathbf{K}_p(kd)\right)}{2p+2q+1}\times\left({}_n\mathbf{A}_q(kd)-i_n\mathbf{K}_q(kd)\right), \quad \begin{cases} m=0,1,\ldots,N \\ n=0,1,\ldots,N \end{cases}, \tag{37}$$

$$\mathbf{b}(m+1)=-\sum_{p=0}^{P}\frac{\left({}_m\mathbf{A}_p(kd)-i_m\mathbf{K}_p(kd)\right)}{2p+1}\left(\frac{a}{d}\right)^{2p+1}, \quad m=0,1,\cdots,N, \tag{38}$$

$$\mathbf{a}(n+1)=A_n, \quad n=0,1,\ldots,N. \tag{39}$$

A truncation limit of $N=2kd$ was used for the calculations in this paper. For larger values of N, no discernable difference could be seen in the plots.

F. Solution of the power series coefficients for a line source in a finite baffle

In the case of two line sources at a distance of a from either side of the center of a finite baffle of width $2d$, the surface velocity distribution is given by

$$\Phi(x)=\begin{cases}d\delta(x-a), & 0\le x\le d\\ d\delta(x+a), & -d\le x\le 0\end{cases}, \tag{40}$$

where δ is the Dirac δ function. Inserting this into Eq. (32) and truncating the infinite series limit to order N, yields the following set of $N+1$ simultaneous equations

$$\sum_{n=0}^{N} A_n \int_d^d I_m(x) I_n(x) dx = -d \int_{-d}^{0} \delta(x+a) I_m(x) dx - d \int_0^d \delta(x-a) I_m(x) dx, \quad m = 0, 1, \ldots, N, \tag{41}$$

where $I_m(x)$ and $I_n(x)$ are given by Eqs. (34) and (35), respectively. Integrating over w and using the property of the Dirac δ function yields the same matrix equations as Eqs. (36) to (39) except that

$$\mathbf{b}(m+1) = -\sum_{p=0}^{P} \left({}_m\mathbf{A}_p(kd) - i_m\mathbf{K}_p(kd) \right) \left(\frac{a}{d}\right)^{2p}. \tag{42}$$

In the limiting case of a line source at the center of a finite baffle of width $2d$, we let $a \to 0$ so that

$$\mathbf{b}(m+1) = -({}_m\mathbf{A}_0(kd) - i_m\mathbf{K}_0(kd)). \tag{43}$$

A truncation limit of $N = 2kd$ was used for the calculations in this paper. For larger values of N, no discernable difference could be seen in the plots.

G. Far-field pressure for a rigid strip in a finite baffle

The far-field pressure distribution for the rigid strip in a finite baffle is given by the dipole boundary integral of Eq. (6), but using the far-field Green's function in spherical-rectangular coordinates:

$$\tilde{p}(r,\theta) = \int_{-d}^{d} (\tilde{p}_+(x_0,0) - \tilde{p}_-(x_0,0)) \times \frac{\partial}{\partial z_0} g(r,\theta|x_0,z_0)|_{z_0=0} dx_0, \tag{44}$$

In the far field, the Hankel function of Eq. (10) is simplified by

$$H_0^{(1)}(kR)\Big|_{R\to\infty} = \sqrt{\frac{2}{\pi kR}} e^{-i(kR-\pi/4)}, \tag{45}$$

together with the substitutions $x = r\ \sin\theta$ and $z = r\ \cos\theta$, which enable the square root to be eliminated due to the dominance of the r terms so that the far-field Green's function is given by

$$g(r,\theta|w_0,z_0) = \frac{1}{2\sqrt{2\pi kr}} e^{-ik(r - x_0 \sin\theta - z_0\cos\theta) + i\pi/4} \tag{46}$$

Inserting Eqs. (5) and (46) into Eq. (44) and integrating over the surface using Eq. (14) yields

$$\tilde{p}(r,\theta) = ka\rho c\tilde{u}_0 \sqrt{\frac{2a}{\pi r}} e^{-i(kr-\pi/4)} D(\theta), \tag{47}$$

where the directivity function $D(\theta)$ is given by

$$D(\theta) = \frac{d}{2a}\sqrt{\frac{\pi}{ka}} \cos\theta \sum_{n=0}^{N} A_n \Gamma\left(n+\tfrac{3}{2}\right) \frac{2^{n+1} J_{n+1}(kd\sin\theta)}{(kd\sin\theta)^{n+1}}. \tag{48}$$

Directivity patterns of a rigid strip in free space and a finite baffle of width $d = 2a$ is plotted in Fig. 2. The on-axis pressure is evaluated using the property $J_{n+1}(x)/x^{n+1}|_{n\to 0} = (2^{n+1}(n+1)!)^{-1}$ to give

$$D(0) = \frac{d}{2a}\sqrt{\frac{\pi}{ka}} \sum_{n=0}^{N} A_n \frac{\Gamma\left(n+\frac{3}{2}\right)}{\Gamma(n+2)}, \tag{49}$$

The on-axis response $20\ \log_{10}(D(0))$ of a rigid strip in a finite baffle of width d = 2a is plotted in Fig. 3 along with those of a rigid strip in free space and an infinite baffle. The on-axis response of a line source is plotted in Fig. 4.

H. Radiation impedance for a rigid strip in a finite baffle

The total radiation force per unit length L is the integral of the pressure from Eq. (5) over the surface of the strip on both sides

$$\frac{\tilde{F}_0}{L} = \int_{-a}^{a} (\tilde{p}_+(x_0,0) - \tilde{p}_-(x_0,0)) dx_0 = 4a\rho c\tilde{u}_0 \sum_{n=0}^{N} A_n {}_2F_1\left(-n-\tfrac{1}{2},\tfrac{1}{2},\tfrac{3}{2},\tfrac{a^2}{d^2}\right) \tag{50}$$

The specific radiation impedance per side is then given by

$$Z_s = \frac{\tilde{F}_0}{2\tilde{U}_0} = \frac{\tilde{F}_0}{4La\tilde{u}_0} = R_s + iX_s \tag{51}$$

where $\tilde{U}_0 = 2La\tilde{u}_0$ is the volume velocity per unit length L and R_s is the specific radiation resistance per side given by

$$R_s = \rho c \Re\left(\sum_{n=0}^{N} A_n {}_2F_1\left(-n-\tfrac{1}{2},\tfrac{1}{2},\tfrac{3}{2},\tfrac{a^2}{d^2}\right)\right) \tag{52}$$

and X_s is the radiation reactance per side given by

$$X_s = \rho c \Im\left(\sum_{n=0}^{N} A_n {}_2F_1\left(-n-\tfrac{1}{2},\tfrac{1}{2},\tfrac{3}{2},\tfrac{a^2}{d^2}\right)\right) \tag{53}$$

In the case of a strip in free space without a baffle, where $a = d$, these expressions become

$$R_s = \rho c \frac{\sqrt{\pi}}{2} \Re\left(\sum_{n=0}^{N} A_n \frac{\Gamma(n+\frac{3}{2})}{\Gamma(n+2)}\right) \approx \frac{\pi^2 k^3 a^3}{32}\rho c, \quad ka < 0.3 \tag{54}$$

$$X_s = \rho c \frac{\sqrt{\pi}}{2} \Im\left(\sum_{n=0}^{N} A_n \frac{\Gamma(n+\frac{3}{2})}{\Gamma(n+2)}\right) \approx \frac{\pi ka}{4}\rho c, \quad ka < 0.3 \tag{55}$$

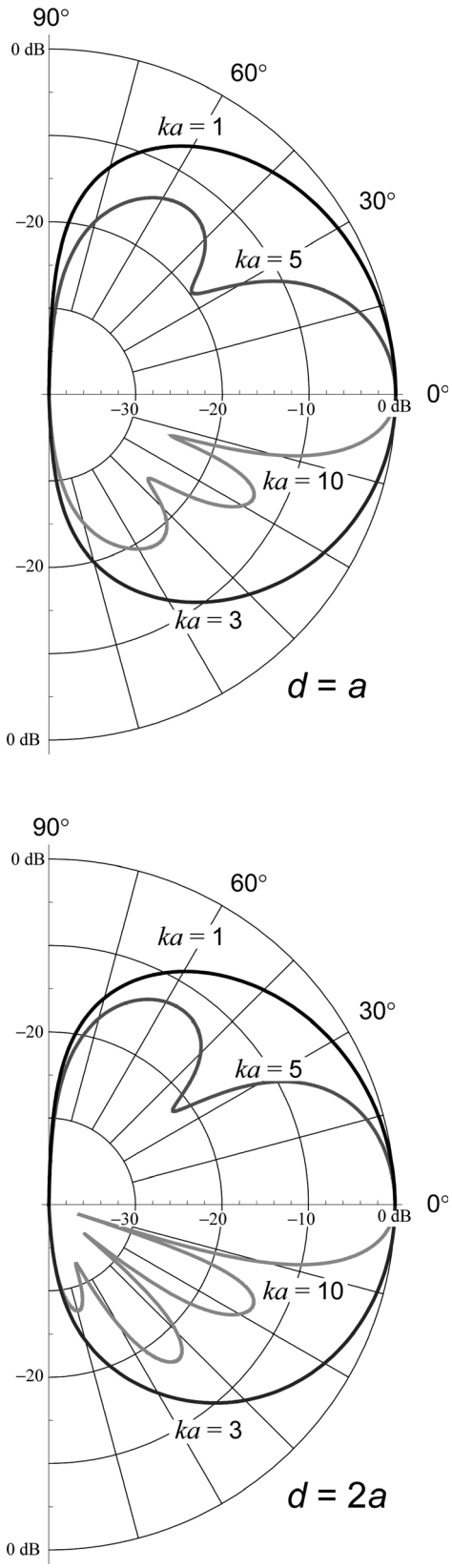

FIG. 2. Directivity patterns of a rigid strip in a baffle of width $d = 2a$ and in free space.

The radiation resistance and reactance of a rigid strip in a finite baffle of width $d = 2a$ is plotted in Fig. 5 along with those of a rigid strip in an infinite baffle and free space. The radiation conductance and susceptance of a rigid strip in free space are plotted along with those of a resilient strip in free space in Fig. 8.

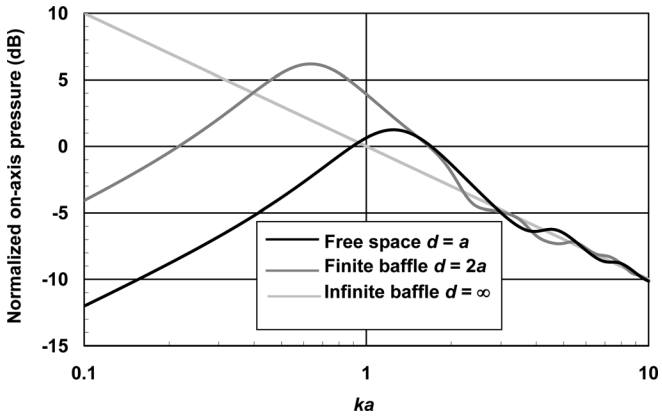

FIG. 3. On-axis response of a rigid strip in finite baffles of various widths, where $d = a$, $2a$, and ∞.

III. RESILIENT STRIP IN FREE SPACE

A. Far-field pressure for a resilient strip in free space

The far-field pressure for a resilient strip of width $2a$ in free space with a uniform surface pressure distribution is obtained by the same procedure as before but using $\tilde{p}_+(x_0, 0) = -\tilde{p}_-(x_0, 0) = \tilde{p}_0/2$ in Eq. (44) instead of Eq. (5) to obtain

$$\tilde{p}(r, \theta) = \tilde{p}_0 \sqrt{\frac{a}{2\pi r}} e^{-i(kr-\pi/4)} D(\theta), \tag{56}$$

where the directivity function $D(\theta)$ is given by

$$D(\theta) = \frac{\sin(ka \sin\theta)}{\sqrt{ka} \sin\theta} \cos\theta. \tag{57}$$

Directivity patterns of a resilient strip in free space are plotted in Fig. 6. The on-axis pressure is given by $D(0) = \sqrt{ka}$, which is plotted in Fig. 7 along with the on-axis response of a resilient strip in an infinite baffle.

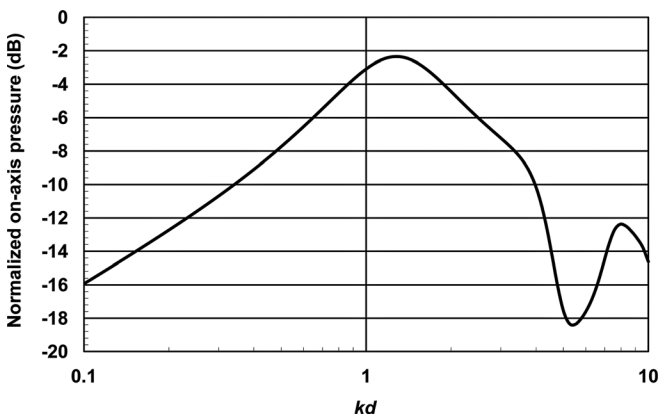

FIG. 4. On-axis response of a line source in a finite baffle of width $2d$.

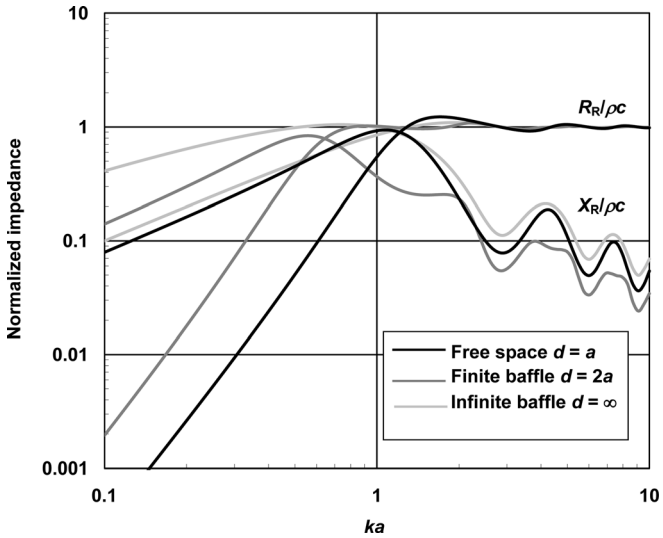

FIG. 5. Normalized radiation impedance of a rigid strip in finite baffles of various widths, where $d=a$, $2a$, and ∞.

B. Radiation admittance for a resilient strip in free space

In the case of a resilient strip in free space, we replace Eq. (5) with $\tilde{p}_+(x_0,0)=-\tilde{p}_-(x_0,0)=\tilde{p}_0/2$. Inserting this together with Eqs. (1) and (11) into Eq. (6) and integrating over x_0 yields

$$\tilde{p}(x,z)=\frac{\tilde{p}_0}{2\pi}\int_{-\infty}^{\infty}\frac{\sin k_x a}{k_x}e^{-i(k_x x+k_z|z|)}dk_x, \tag{58}$$

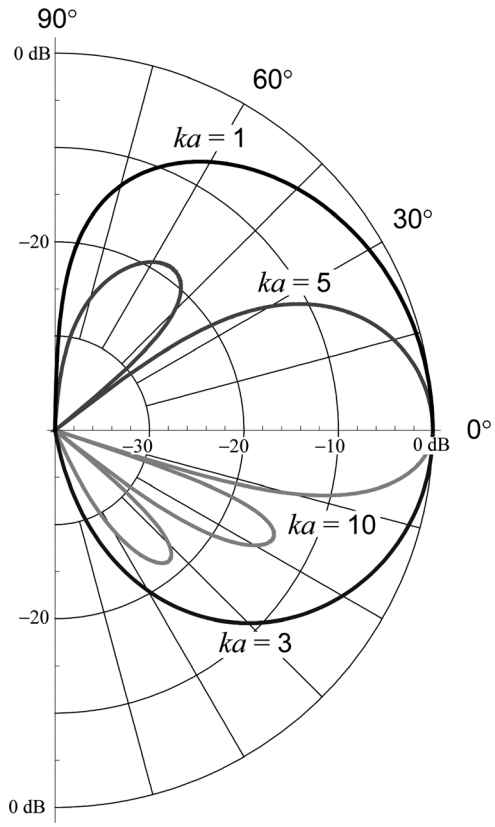

FIG. 6. Directivity patterns of a resilient strip in free space.

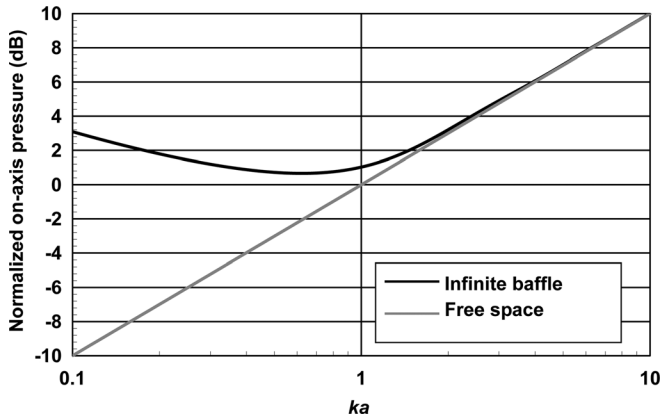

FIG. 7. On-axis responses of a resilient strip in free space and in an infinite baffle.

The total volume velocity per unit length L is then given by

$$\begin{aligned}\tilde{U}_0&=-\frac{L}{ik\rho c}\int_{-a}^{a}\frac{\partial}{\partial z}\tilde{p}(x,z)|_{z=0}dx\\&=\frac{2L\tilde{p}_0}{\pi k\rho c}\int_0^{\infty}\left(\frac{\sin k_x a}{k_x}\right)^2 k_z dk_x,\end{aligned} \tag{59}$$

With the substitution $k_x=kt$, the infinite integral can be split into real and imaginary parts. The specific radiation admittance per side is

$$Y_s=\frac{\tilde{U}_0}{aL\tilde{p}_0}=G_s-iB_s, \tag{60}$$

where G_s is the specific radiation conductance per side given by

$$\begin{aligned}G_s&=\frac{2ka}{\pi\rho c}\int_0^1\left(\frac{\sin kat}{kat}\right)^2\sqrt{1-t^2}dt\\&=\rho c\left(\frac{J_0(2ka)-1}{2ka}+ka\,{}_1F_2\left(\frac{1}{2};\frac{3}{2},2;-k^2a^2\right)\right)\\&\approx\rho c\frac{ka}{2},\quad ka<0.5,\end{aligned} \tag{61}$$

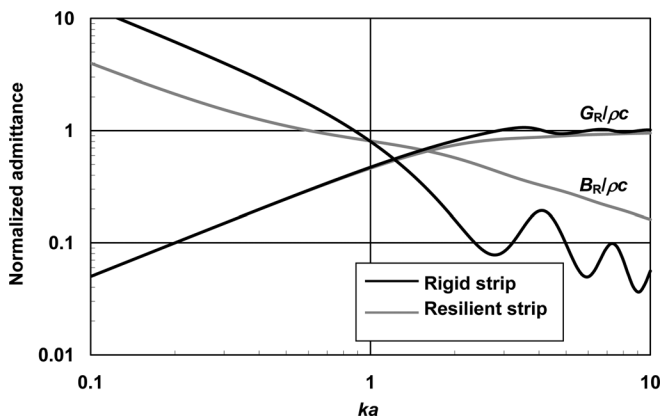

FIG. 8. Normalized radiation admittances of rigid and resilient strips in free space.

and B_s is the specific radiation susceptance per side given by

$$B_s = \frac{2ka}{\pi\rho c}\int_1^\infty \left(\frac{\sin kat}{kat}\right)^2 \sqrt{t^2-1}\,dt = \rho c \frac{1}{2ka}\left(\frac{4}{\pi} - \frac{1}{2} + \frac{1}{2}G^{2,2}_{3,5}\left(k^2a^2 \middle| \begin{matrix} 1,1,\frac{3}{2} \\ 1,1,0,0,\frac{1}{2} \end{matrix}\right)\right). \quad (62)$$

where G is the Meijer G-function. The normalized conductance and susceptance of a resilient strip in free space are plotted in Fig. 8 along with those of a rigid strip in free space.

IV. RESILIENT STRIP IN AN INFINITE BAFFLE

A. Boundary conditions

The strip of width $2a$ shown in Fig. 1 is mounted in an infinite baffle in the xy plane with its line of symmetry on the y axis so that the limits of the baffle shown at d and - d are no longer applicable. The infinitesimally thin membrane-like resilient strip is assumed to be perfectly flexible, has zero mass, and is free at its outer edges. It is driven by a uniformly distributed harmonically varying pressure $\tilde{p}_0$ and thus radiates sound from both sides into a homogeneous loss-free acoustic medium. In fact, there need not be a strip present at all and instead the driving pressure could be acting upon the air particles directly. However, for expedience, the area over which this driving pressure is applied shall be referred to as a strip from here onward. On the surface of the strip and baffle, the following boundary conditions apply:

$$\frac{\partial}{\partial z}\tilde{p}(x,z)|_{z=0+} = \begin{cases} -ik\rho c\tilde{u}(x,z)|_{z=0}, & -a \le x \le a \\ 0, & -\infty \le x < a, \quad a < x \le \infty \end{cases} \quad (63)$$

where

$$\tilde{u}(x,z)|_{z=0} = \frac{\tilde{p}_0}{\rho c}\sum_{n=0}^{\infty} A_n \left(1 - \frac{x^2}{a^2}\right)^{n-\frac{1}{2}}, \quad (64)$$

where A_n are the as yet unknown power series coefficient that will be calculated by means of a set of simultaneous equations in matrix form and k is the wave number given by

$$k = \frac{\omega}{c} = \frac{2\pi}{\lambda}, \quad (65)$$

where ω is the angular frequency of excitation, ρ is the density of the surrounding medium, c is the speed of sound in that medium, and λ is the wavelength. The annotation ~ denotes a harmonically time-varying quantity and replaces the factor $e^{i\omega t}$. It is worth noting that the index of the first term of the expansion ($m=0$) is equal to $-1/2$, in order to satisfy the boundary condition of infinite velocity at the perimeter, as determined by Rayleigh.[23] The same expansion can be applied to any velocity distribution, provided that the velocity is either infinite or zero at the perimeter. For example, in the case of an infinite membrane strip with a clamped edge, the index of the first term would be equal to $+1/2$.

On the front and rear surfaces of the strip, the pressures are $\tilde{p}_+$ and $\tilde{p}_-$, respectively, which are given by

$$\tilde{p}(x,z)_{z=0+} = -\tilde{p}(x,z)_{z=0-} = \frac{\tilde{p}_0}{2}. \quad (66)$$

B. Boundary integral

The nearfield pressure is given by the monopole Rayleigh integral or monopole part of the Kirchhoff–Helmholtz boundary integral taking into account the double strength source

$$\tilde{p}(x,z) = 2\int_{-a}^{a} \frac{\partial}{\partial z_0}\tilde{p}(x_0,z)|_{z=0+} g(x,z|x_0,z_0)|_{z_0=0} dx_0, \quad (67)$$

where the Green's function in rectangular coordinates is given by Eq. (11).

C. Formulation of the coupled equation for a resilient strip

Inserting Eqs. (63), (64), and (11) into Eq. (6) and integrating over x_0 gives

$$\tilde{p}(x,z) = -\frac{ka\tilde{p}_0}{\sqrt{\pi}}\sum_{n=0}^{\infty} A_n 2^{n-1}\Gamma\left(n+\tfrac{1}{2}\right) \times \int_{-\infty}^{\infty} \frac{J_n(k_x a)}{(k_x a)^n}\frac{e^{-i(k_x x + k_z|z|)}}{k_z}dk_x, \quad (68)$$

where the following differential-integral solution has been applied[22]

$$\int_{-a}^{a}\left(1-\frac{x_0^2}{a^2}\right)^{n-\frac{1}{2}} e^{ik_x x_0}dx_0 = 2\int_0^a \cos k_x x_0 \left(1-\frac{x_0^2}{a^2}\right)^{n-\frac{1}{2}} dx_0. = \sqrt{\pi}a2^n\Gamma\left(n+\tfrac{1}{2}\right)\frac{J_n(k_x a)}{(k_x a)^n} \quad (69)$$

Applying the boundary condition of Eq. (66) leads to the coupled equation

$$\sum_{n=0}^{\infty} A_n I_n(x) = -\Phi(x) = -1, \quad (70)$$

which is to be solved for the power series coefficients A_n. Letting $k_x = kt$, the integral $I_n(x)$ can be split into two parts

$$I_n(x) = I_{nR}(x) + iI_{nI}(x), \quad (71)$$

where the real part is given by

$$I_{nR}(x) = \frac{2^{n+1}\Gamma\left(n+\frac{1}{2}\right)ka}{\sqrt{\pi}}\int_0^1 \frac{J_n(kat)}{(kat)^n}\frac{\cos kxt}{\sqrt{1-t^2}}dt, \quad (72)$$

and the imaginary part is given by

$$I_{nI}(x) = \frac{2^{n+1}\Gamma\left(n+\frac{1}{2}\right)ka}{\sqrt{\pi}}\int_1^\infty \frac{J_n(kat)}{(kat)^n}\frac{\cos kxt}{\sqrt{t^2-1}}dt. \tag{73}$$

Using the same expansions and contour of integration as shown in the appendix for the rigid strip in a finite baffle, the solutions to these integrals can be shown to be

$$I_{nR}(x) = 2\sum_{m=0}^{\infty}\sum_{r=0}^{\infty}\frac{(-1)^{m+r}\Gamma\left(n+\frac{1}{2}\right)\Gamma(m+r+\frac{1}{2})}{(2m)!r!(n+r)!(m+r)!} \times\left(\frac{ka}{2}\right)^{2m+2r+1}\left(\frac{2x}{a}\right)^{2m}, \tag{74}$$

$$\begin{aligned} I_{nI}(x) = -\frac{2}{\pi}\sum_{m=0}^{\infty}\Bigg\{&\sum_{r=0}^{\infty}\frac{(-1)^{m+r}\Gamma\left(n+\frac{1}{2}\right)\Gamma(m+r+\frac{1}{2})}{(2m)!r!(n+r)!(m+r)!} \times\left(\frac{ka}{2}\right)^{2m+2r+1}\times\left(2\ln\left(\frac{ka}{2}\right)+\psi(m+r+\tfrac{1}{2})\right.\\ &\left.-\psi(m+r+1)-\psi(r+1)-\psi(n+r+1)\right)\\ &-\sum_{r=0}^{n-1}\frac{(-1)^m(n-r-1)!\Gamma\left(n+\frac{1}{2}\right)\Gamma(m+r-n+\frac{1}{2})}{(2m)!r!(m+r-n)!} \times\left(\frac{ka}{2}\right)^{2m+2r-2n+1}\Bigg\}\left(\frac{2x}{a}\right)^{2m} \end{aligned} \tag{75}$$

D. Solution of the power series coefficients for a resilient strip in an infinite baffle

Equations (74) and (75) are both expansions in $(2x/a)^{2m}$. Hence, in order to solve for the expansion coefficients, it is useful to express the strip pressure distribution $\Phi(x)$ as a function of $(2x/a)^{2m}$, so that

$$\Phi(x)|_{d=a} = 1 = \sum_{m=0}^{\infty}\delta_{m0}\left(\frac{2x}{a}\right)^{2m}, \quad 0\le x\le a, \tag{76}$$

where δ_{m0} is the Kronecker δ function as defined in Eq. (23). Inserting Eqs. (71), (74), (75), and (76) in Eq. (70) and equating the coefficients of $(2x/a)^{2m}$ yields the following $(N+1)\times(N+1)$ matrix equation

$$\mathbf{M}\cdot\mathbf{a} = \mathbf{b} \Rightarrow \mathbf{a} = \mathbf{M}^{-1}\cdot\mathbf{b}, \tag{77}$$

where the matrix $\mathbf{M}$ and vectors $\mathbf{a}$ and $\mathbf{b}$ are given by

$$\mathbf{M}(m+1,n+1) = {}_n\mathbf{C}_m(ka) - i_n\mathbf{I}_m(ka), \quad \begin{cases} m=0,1,\ldots,N \\ n=0,1,\ldots,N \end{cases}, \tag{78}$$

$$\mathbf{b}(m+1) = -\delta_{m0}, \quad m=0,1,\ldots,N, \tag{79}$$

$$\mathbf{a}(n+1) = A_n, \quad n=0,1,\ldots,N, \tag{80}$$

and the infinite power series limits have been truncated to order N. The two-dimensional rectangular monopole wave functions ${}_n\mathbf{C}_m$ and ${}_n\mathbf{I}_m$ are defined by

$${}_n\mathbf{C}_m(ka) = 2\sum_{r=0}^{N}\frac{(-1)^{m+r}\Gamma\left(n+\frac{1}{2}\right)\Gamma(m+r+\frac{1}{2})}{(2m)!r!(n+r)!(m+r)!} \times\left(\frac{ka}{2}\right)^{2m+2r+1}, \tag{81}$$

$$\begin{aligned} {}_n\mathbf{I}_m(ka) = &\frac{2}{\pi}\sum_{r=0}^{N}\frac{(-1)^{m+r}\Gamma\left(n+\frac{1}{2}\right)\Gamma(m+r+\frac{1}{2})}{(2m)!r!(n+r)!(m+r)!} \times\left(\frac{ka}{2}\right)^{2m+2r+1}\times\left(2\ln\left(\frac{ka}{2}\right)+\psi(m+r+\tfrac{1}{2})\right.\\ &\left.-\psi(m+r+1)-\psi(r+1)-\psi(n+r+1)\right)\\ &-\frac{2}{\pi}\sum_{r=0}^{n-1}\frac{(-1)^m(n-r-1)!\Gamma\left(n+\frac{1}{2}\right)\Gamma(m+r-n+\frac{1}{2})}{(2m)!r!(m+r-n)!} \times\left(\frac{ka}{2}\right)^{2m+2r-2n+1}. \end{aligned} \tag{82}$$

A truncation limit of $N=2ka$ was used for the calculations in this paper. For larger values of N, no discernable difference could be seen in the plots.

E. Far-field pressure for a resilient strip in an infinite baffle

The far-field pressure distribution for the resilient strip in an infinite baffle is given by the monopole boundary integral of Eq. (67) but using the far-field Green's function in spherical-rectangular coordinates:

$$\tilde{p}(r,\theta) = 2\int_{-a}^{a}\frac{\partial}{\partial z_0}\tilde{p}(x_0,z)|_{z=0+}g(r,\theta|x_0,z_0)|_{z_0=0}dx_0, \tag{83}$$

where the far-field Green's function is given by Eq. (46). Inserting Eqs. (46), (63), and (64) into Eq. (83) and integrating over the surface using Eq. (69) yields

$$\tilde{p}(r,\theta) = \tilde{p}_0\sqrt{\frac{a}{2\pi r}}e^{-i(kr-\pi/4)}D(\theta), \tag{84}$$

where the directivity function $D(\theta)$ is given by

$$D(\theta) = -i\sqrt{\pi ka}\sum_{n=0}^{N}A_n\Gamma\left(n+\tfrac{1}{2}\right)\frac{2^nJ_n(ka\sin\theta)}{(ka\sin\theta)^n}. \tag{85}$$

Directivity patterns of a resilient strip in an infinite baffle are plotted in Fig. 9. The on-axis pressure is evaluated using the property $J_n(x)/x^n|_{n\to0} = (2^n n!)^{-1}$ to give

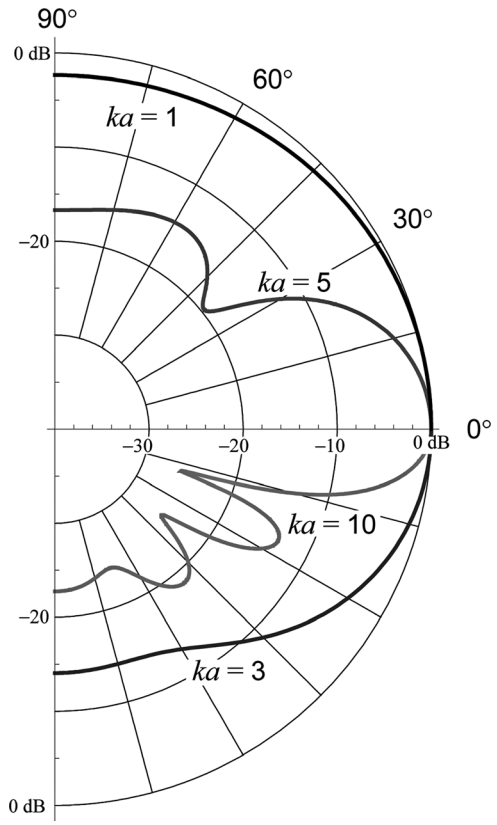

FIG. 9. Directivity patterns of a resilient strip in an infinite baffle.

$$D(0) = -i\sqrt{\pi ka}\sum_{n=0}^{N} A_n \frac{\Gamma\left(n+\frac{1}{2}\right)}{\Gamma(n+1)}, \tag{86}$$

which at low and high frequencies can be approximated by

$$D(0) \approx \begin{cases} \sqrt{ka}, & ka > 2 \\ -\dfrac{\pi}{2\sqrt{ka}\ln(ka/4)}, & ka \to 0 \end{cases} \tag{87}$$

The on-axis responses $20\log_{10}(D(0))$ of a resilient strip in an infinite baffle is plotted in Fig. 7 along with that of a resilient strip in free space.

F. Radiation admittance for a resilient strip in an infinite baffle

The average velocity is the integral of the velocity from Eq. (64) over the width of the strip divided by the width

$$\tilde{u}_0 = \frac{1}{2a}\int_{-a}^{a} \tilde{u}(x,z)|_{z=0} dx_0 = \frac{\sqrt{\pi}\tilde{p}_0}{2\rho c}\sum_{n=0}^{\infty} A_n \frac{\Gamma\left(n+\frac{1}{2}\right)}{\Gamma(n+1)} \tag{88}$$

The specific radiation admittance per side is then given by

$$Y_s = \frac{2\tilde{u}_0}{\tilde{p}_0} = G_s + iB_s \tag{89}$$

where G_s is the specific radiation conductance per side given by

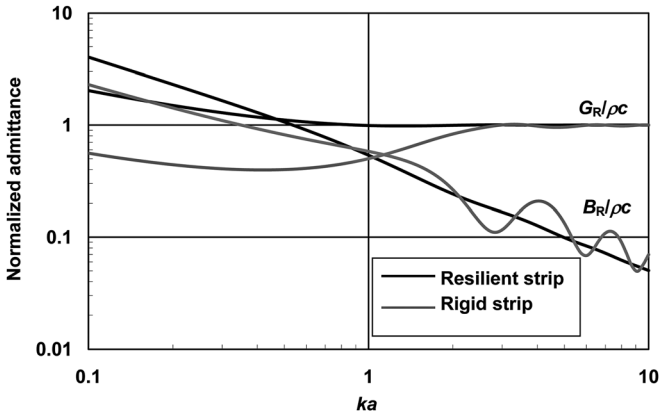

FIG. 10. Normalized radiation admittances of resilient and rigid strips in an infinite baffle.

$$G_s = \frac{\sqrt{\pi}}{\rho c}\Re\left(\sum_{n=0}^{N} A_n \frac{\Gamma\left(n+\frac{1}{2}\right)}{\Gamma(n+1)}\right) \tag{90}$$

and B_s is the radiation susceptance per side given by

$$B_s = \frac{\sqrt{\pi}}{\rho c}\Im\left(\sum_{n=0}^{N} A_n \frac{\Gamma\left(n+\frac{1}{2}\right)}{\Gamma(n+1)}\right) \tag{91}$$

Then R_s is the radiation resistance per side is then given by

$$R_s = \frac{G_s}{G_s^2 + B_s^2} \approx ka, \quad ka < 0.3 \tag{92}$$

and B_s is the radiation susceptance per side given by

$$X_s = \frac{B_s}{G_s^2 + B_s^2} \approx -\frac{2ka}{\pi}\left(\ln\left(\frac{ka}{4}\right) + \gamma\right), \quad ka < 0.3 \tag{93}$$

where $\gamma = 0.5772$ is Euler's constant. The radiation resistance and reactance of a resilient strip in an infinite baffle are plotted along with those of a rigid strip in an infinite baffle in Fig. 10.

V. RIGID STRIP IN AN INFINITE BAFFLE

A. Far-field pressure for a rigid strip in an infinite baffle

The far-field pressure for a rigid strip of width $2a$ in an infinite baffle with a uniform surface velocity distribution is obtained by same procedure as before but using $\tilde{u}(x,z)|_{z=0} = \tilde{u}_0$ in Eq. (83) instead of Eq. (64) to obtain

$$\tilde{p}(r,\theta) = -ika\rho c\tilde{u}_0\sqrt{\frac{2a}{\pi r}}e^{-i(kr-\pi/4)}D(\theta), \tag{94}$$

where the directivity function $D(\theta)$ is given by

$$D(\theta) = \frac{\sin(ka\sin\theta)}{(ka)^{3/2}\sin\theta}. \tag{95}$$

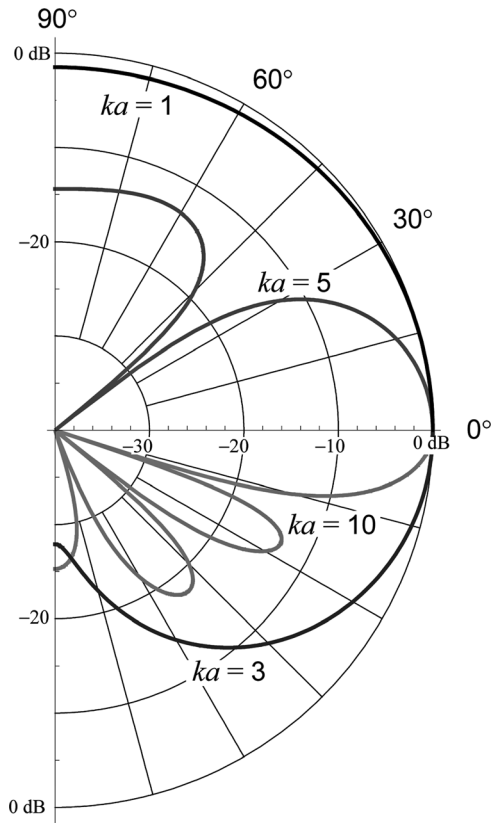

FIG. 11. Directivity patterns of a rigid strip in an infinite baffle.

Directivity patterns of a rigid strip in an infinite baffle are plotted in Fig. 11. The on-axis pressure is given by $D(0) = 1/\sqrt{ka}$, as shown in Fig. 3.

B. Radiation impedance for a rigid strip in an infinite baffle

In the case of a rigid strip in an infinite baffle, we replace Eq. (64) with $\tilde{u}(x,z)|_{z=0} = \tilde{u}_0$. Inserting this together with Eqs. (63) and (11) into Eq. (67) and integrating over x_0 yields

$$\tilde{p}(x,z) = -k\rho c\tilde{u}_0 \frac{1}{\pi}\int_{-\infty}^{\infty} \frac{\sin k_x a}{k_x}\frac{e^{-i(k_x x + k_z|z|)}}{k_z}dk_x, \tag{96}$$

The total radiation force per length L on both sides is then given by

$$\frac{\tilde{F}_0}{L} = -2\int_{-a}^{a}\tilde{p}(x,z)|_{z=0}dx = 8k\rho c\tilde{u}_0\frac{1}{\pi}\int_0^{\infty}\left(\frac{\sin k_x a}{k_x}\right)^2\frac{1}{k_z}dk_x. \tag{97}$$

With the substitution $k_x = kt$, the infinite integral can be split into real and imaginary parts. The specific radiation impedance per side is

$$Z_s = \frac{\tilde{F}_0}{4aL\tilde{u}_0} = R_s + iX_s, \tag{98}$$

where R_s is the specific radiation resistance per side given by

$$R_s = \rho c\frac{2ka}{\pi}\int_0^1\left(\frac{\sin kat}{kat}\right)^2\frac{1}{\sqrt{1-t^2}}dt = \rho cka\,{}_1F_2\left(\frac{1}{2};\frac{3}{2},2;-k^2a^2\right) \approx \rho cka, ka < 0.5, \tag{99}$$

and X_s is the specific radiation reactance per side given by

$$X_s = \rho c\frac{2ka}{\pi}\int_1^{\infty}\left(\frac{\sin kat}{kat}\right)^2\frac{1}{\sqrt{t^2-1}}dt = \rho c\frac{1}{2ka}G^{2,1}_{2,4}\left(k^2a^2\middle|\begin{matrix}1,\frac{3}{2}\\1,1,0,\frac{1}{2}\end{matrix}\right) \approx \rho c\frac{2ka}{\pi}\left(\frac{3}{2}-\gamma-\ln(ka)\right), ka < 0.5, \tag{100}$$

where F is the hypergeometric function, G is the Meijer G function, and $\gamma = 0.5772$ is Euler's constant. The radiation resistance and reactance of a rigid strip in an infinite baffle are plotted along with those of a resilient strip in an infinite baffle in Fig. 10.

VI. RELATIONSHIP BETWEEN A RIGID STRIP IN AN INFINITE BAFFLE AND A RESILIENT STRIP IN FREE SPACE

Suppose that the radiation resistance and reactance of a rigid strip in an infinite baffle are denoted by R_s and X_s, respectively, and G_s and B_s are the radiation conductance and susceptance, respectively, of a resilient strip in free space defined in Eqs. (61) and (62). Then

$$(\rho c)^2\frac{d}{d(ka)}kaG_s(ka) = R_s(ka) = \rho cka\,{}_1F_2\left(\frac{1}{2};\frac{3}{2},2;-k^2a^2\right), \tag{101}$$

or

$$G_s(ka) = \frac{1}{ka(\rho c)^2}\left(\int R_s(ka)d(ka) - \frac{1}{2}\right), \tag{102}$$

and

$$(\rho c)^2\frac{d}{d(ka)}kaB_s(ka) = X_s(ka) = \rho c\frac{1}{2ka}G^{2,1}_{2,4}\left(k^2a^2\middle|\begin{matrix}1,\frac{3}{2}\\1,1,0,\frac{1}{2}\end{matrix}\right) \tag{103}$$

or

$$B_s(ka) = \frac{1}{ka(\rho c)^2}\left(\int X_s(ka)d(ka) - \frac{1}{2} + \frac{4}{\pi}\right). \tag{104}$$

VII. DISCUSSION

Like a rigid disk in a finite baffle, the on-axis response of a rigid strip in a finite baffle shown in Fig. 3 exhibits peaks and dips due to constructive and destructive interference from the rear wave. However, these features are less pronounced, even in the limiting case of a line source shown in Fig. 4, which suggests that a transducer with a large aspect ratio in a finite baffle is more desirable than a circular one. The far-field pressure of a plane wave radiator (e.g., oscillating infinite wall or piston radiating into an infinite tube) is proportional to the velocity of the radiator, whereas the far-field pressure of a circular or finite piston in an infinite baffle is proportional to the acceleration (i.e., first time derivative of the velocity) of the radiator because the waves are spreading out three-dimensionally as opposed to one dimensionally. In the case of an infinite strip in an infinite baffle, the waves spread out two dimensionally so that the far-field pressure is proportional to the half derivative of the velocity, which explains why the response is proportional to the inverse square-root of the frequency when the acceleration is constant. For a circular or finite piston, the response is flat under constant acceleration. Hence, the response of the infinite ribbon is tilted toward the low frequencies with a slope of 3 dB/octave. This tilt is applied to all of the on-axis responses (see Figs. 3, 4, and 7) when compared with circular radiators of the same type.

The fact that infinite strips radiate more power at low frequencies than circular disks is also reflected in the impedance and admittance curves (see Figs. 5, 8, and 10). For instance, the radiation resistance of a rigid strip in free space is proportional to k^3a^3 but for a circular rigid piston it is proportional to k^4a^4. Furthermore, the radiation conductance of a resilient strip in free space and the radiation resistance of a resilient or rigid strip in an infinite baffle are all proportional to ka, whereas the corresponding quantities for circular radiators are all proportional to k^2a^2.

As with circular radiators, nulls in the far-field directivity patterns occur when either the velocity or pressure is uniform over the radiating surface and the same quantity that is uniform over the surface is also zero in the surrounding plane. This is demonstrated in Figs. 6 and 11. Although the remaining directivity patterns, which result from mixed boundary conditions over the radiators and their surrounding planes, do show large variations in pressure with angle, no nulls occur (see Figs. 2 and 9).

VIII. CONCLUSIONS

Methods previously used to analyze circular radiators have been extended to four kinds of infinite strip, which involve more complicated wave functions. Although both types of problem are two dimensional from a computational point of view, the circular radiators are physically three dimensional, albeit axisymmetrical. Hence, these solutions provide insight into the differences between two- and three-dimensional sound radiation. It would be interesting to see this method extended to a three-dimensional problem of practical importance such as sound radiation from a rectangular piston in a finite baffle or free space. The authors have verified that expansions similar to those derived by Stenzel[19] for a rigid rectangular piston in an infinite baffle can be obtained. The results also agree well with those of Bank and Wright,[20] whose findings were obtained somewhat less efficiently than Stenzel using numerical integration.

The two-dimensional rectangular wave functions developed in this paper can be applied to fluid-structure coupled problems such as infinitely long membranes and clamped or simply supported plates.

APPENDIX: SOLUTION OF THE INTEGRALS FOR A RIGID STRIP IN A FINITE BAFFLE

A. Solution of the real integral

The integral of over t in Eq. (18) is solved by applying the following expansions

$$\cos kxt = \sum_{m=0}^{\infty} \frac{(-1)^m (kxt)^{2m}}{(2m)!}. \tag{A1}$$

$$J_{n+1}(kdt) = \sum_{r=0}^{\infty} \frac{(-1)^r}{r!\Gamma(r+n+2)} \left(\frac{kdt}{2}\right)^{2r+n+1}, \tag{A2}$$

together with the integral solution

$$\int_0^1 t^{2m+2r}\sqrt{1-t^2}\,dt = \frac{\sqrt{\pi}\Gamma(m+r+\frac{1}{2})}{4\Gamma(m+r+2)}, \tag{A3}$$

which yields

$$I_{nR}(x) = \frac{1}{2}\sum_{m=0}^{\infty}\sum_{r=0}^{\infty} \frac{(-1)^{m+r}\Gamma\left(n+\frac{3}{2}\right)\Gamma(m+r+\frac{1}{2})}{(2m)!r!(n+r+1)!(m+r+1)!} \times \left(\frac{kd}{2}\right)^{2m+2r+1}\left(\frac{2x}{d}\right)^{2m}. \tag{A4}$$

B. Solution of the imaginary integral

The following procedure converts the infinite limit of the integral in Eq. (19) into a finite one. First, the integral is converted into a form that can be integrated in the complex plane. The Bessel function $J_{n+1}(t)$ can be written in terms of the following pair of complex conjugate functions:

$$J_{n+1}(kdt) = \frac{H_{n+1}^{(1)}(kdt) + H_{n+1}^{(2)}(kdt)}{2}, \tag{A5}$$

where the Hankel functions $H_{n+1}^{(1)}$ and $H_{n+1}^{(2)}$ are defined in terms of Bessel functions of the first and second kind J_n and Y_n, respectively, by

$$H_{n+1}^{(1)}(kdt) = J_{n+1}(kdt) + iY_{n+1}(kdt), \tag{A6}$$

$$H_{n+1}^{(2)}(kdt) = J_{n+1}(kdt) - iY_{n+1}(kdt), \tag{A7}$$

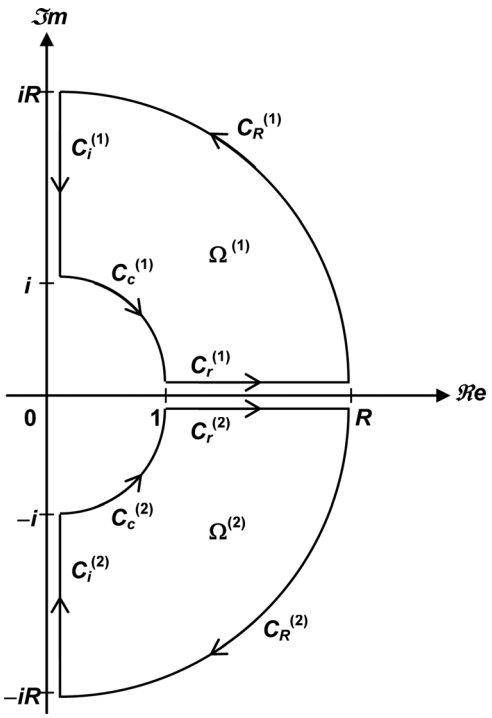

FIG. 12. Contours of integration.

which can be used to separate I_{nI} into two complex conjugate integrals as follows

$$I_{nI}(x) = \frac{I_{nI}^{(1)}(x) + I_{nI}^{(2)}(x)}{2}, \tag{A8}$$

where the complex conjugate integrals are given by

$$I_{nI}^{(1)}(x) = \frac{2^{n+1}\Gamma\left(n+\frac{3}{2}\right)kd}{\sqrt{\pi}} \int_1^\infty \cos kxt \frac{H_{n+1}^{(1)}(kdt)}{(kdt)^{n+1}} \sqrt{t^2-1}\,dt, \tag{A9}$$

$$I_{nI}^{(2)}(x) = \frac{2^{n+1}\Gamma\left(n+\frac{3}{2}\right)kd}{\sqrt{\pi}} \int_1^\infty \cos kxt \frac{H_{n+1}^{(2)}(kdt)}{(kdt)^{n+1}} \sqrt{t^2-1}\,dt. \tag{A10}$$

Referring to the complex t plane of Fig. 11: Directivity patterns of a rigid strip in an infinite baffle.

In Figure 12, the integrals $I_{nI}{}^{(1)}$ and $I_{nI}{}^{(2)}$ can now be evaluated along contours $\Omega^{(1)}$ and $\Omega^{(2)}$, respectively. The contours are defined by

$$\begin{aligned}
&\Omega^{(1)} = t \in (C_r^{(1)} \cup C_R^{(1)} \cup C_i^{(1)} \cup C_c^{(1)}),\\
&C_r^{(1)} = [1, R],\\
&C_R^{(1)} = [Re^{i\vartheta} | 0 \le \vartheta \le \pi/2],\\
&C_i^{(1)} = [iR, i],\\
&C_c^{(1)} = [e^{i\vartheta} | \pi/2 \ge \vartheta \ge 0],\\
&R \to \infty,\\
&\Omega^{(2)} \text{symmetric to } \Omega^{(1)} \text{with respect to the real axis.}
\end{aligned} \tag{A11}$$

1. Contribution of $C_R^{(1)}$ and $C_R^{(2)}$

The contributions along $C_R{}^{(1)}$ and $C_R{}^{(2)}$ vanish for $R \to \infty$ due to the behavior of $H_{n+1}(krt)$ as $|t| \to \infty$.

2. Contribution of $C_i^{(1)}$ and $C_i^{(2)}$

Noting that $\sqrt{t^2-1} = i\sqrt{1-t^2}$, the integral along $C_i{}^{(1)}$ can be written

$$\frac{i2^{n+1}\Gamma\left(n+\frac{3}{2}\right)kd}{\sqrt{\pi}} \int_i^{i\infty} \cos kxt \frac{H_{n+1}^{(1)}(kdt)}{(kdt)^{n+1}} \sqrt{1-t^2}\,dt, \tag{A12}$$

which can be converted into an integral with real limits by substituting $t = is$ as follows:

$$-\frac{2^{n+1}\Gamma\left(n+\frac{3}{2}\right)kd}{\sqrt{\pi}} \int_1^\infty \cos ikxs \frac{H_{n+1}^{(1)}(ikds)}{(ikds)^{n+1}} \sqrt{1+s^2}\,ds. \tag{A13}$$

With help from the following identities:

$$K_\nu(x) = i^{\nu+1}\frac{\pi}{2}H_\nu^{(1)}(ix) \tag{A14}$$

$$\cos ix = \cosh x, \tag{A15}$$

the integral can be written as

$$i\frac{2^{n+2}\Gamma\left(n+\frac{3}{2}\right)kd}{\pi^{3/2}} \int_1^\infty \cosh kxs \frac{K_{n+1}(kds)}{(-kds)^{n+1}} \sqrt{1+s^2}\,ds \tag{A16}$$

where K_ν is the modified or hyperbolic Hankel function. This integral is purely imaginary whereas the original is real valued. Hence, there is zero net contribution along $C_i{}^{(1)}$. The same is true for the contribution along $C_i{}^{(2)}$ where $\sqrt{t^2-1} = -i\sqrt{1-t^2}$.

3. Contribution of $C_c^{(1)}$ and $C_c^{(2)}$

Finally, the contributions along the unity quarter circle segments $C_c{}^{(1)}$ and $C_c{}^{(2)}$ can be calculated by using the substitution $t = e^{i\vartheta}$, so that the contribution along $C_c{}^{(1)}$ becomes

$$\begin{aligned}
&\frac{2^{n+1}\Gamma\left(n+\frac{3}{2}\right)kd}{\sqrt{\pi}(kd)^{n+1}} \Re\left(i\int_{\pi/2}^0 \cos kxe^{i\vartheta} H_{n+1}^{(1)}\left(kde^{i\vartheta}\right)\right.\\
&\left.\times e^{-ni\vartheta}\sqrt{e^{2i\vartheta}-1}\,d\vartheta\right)
\end{aligned} \tag{A17}$$

and likewise the contribution along $C_c{}^{(2)}$ becomes

$$\begin{aligned}
&\frac{2^{n+1}\Gamma\left(n+\frac{3}{2}\right)kd}{\sqrt{\pi}(kd)^{n+1}} \Re\left(i\int_{-\pi/2}^0 \cos kxe^{i\vartheta} H_{n+1}^{(2)}\left(kde^{i\vartheta}\right)\right.\\
&\left.\times e^{-ni\vartheta}\sqrt{e^{2i\vartheta}-1}\,d\vartheta\right),
\end{aligned} \tag{A18}$$

which is equal to Eq. (A17). As there are no poles or zeros within the contours $\Omega^{(1)}$ or $\Omega^{(2)}$, it can be stated that, according to the residue theorem, the sum of the integrals around each of these contours is equal to zero. Therefore, $I_{nI}(x)$ can be written as

$$I_{nI}(x)=\frac{I_{nI}^{(1)}(x)+I_{nI}^{(2)}(x)}{2}=\frac{2^{n+1}\Gamma\left(n+\frac{3}{2}\right)kd}{\sqrt{\pi}(kd)^{n+1}}\times\Re\left(i\int_0^{\pi/2}\cos kxe^{i\vartheta}H_{n+1}^{(1)}\left(kde^{i\vartheta}\right)e^{-ni\vartheta}\sqrt{e^{2i\vartheta}-1}d\vartheta\right). \tag{A19}$$

4. Expansion and solution

We now apply the expansion of Eqs. (A2) and (A1) to Eq. (A19) together with

$$Y_{n+1}(x)=\frac{2}{\pi}\ln\left(\frac{x}{2}\right)J_{n+1}(x)-\frac{1}{\pi}\sum_{r=0}^{n}\frac{(n-r)!}{r!}\left(\frac{x}{2}\right)^{2r-n-1}-\frac{1}{\pi}\sum_{r=0}^{\infty}\frac{(-1)^r(\psi(r+1)+\psi(r+n+2))}{r!(r+n+1)!}\left(\frac{x}{2}\right)^{2r+n+1} \tag{A20}$$

where ψ is the Euler psi function or digamma function. Using the following integral solutions

$$\int_0^{\pi/2}e^{i(2m+2r+1)\vartheta}\sqrt{e^{2i\vartheta}-1}d\vartheta=-\frac{\sqrt{\pi}\Gamma(m+r+\frac{1}{2})}{4\Gamma(m+r+2)}+i\frac{2\sqrt{2}(-1)^{m+r}{}_2F_1(1,m+r+2;m+r+\frac{3}{2};-1)}{2m+2r+1} \tag{A21}$$

$$\begin{aligned}\int_0^{\pi/2}i\vartheta e^{i(2m+2r+1)\vartheta}\sqrt{e^{2i\vartheta}-1}d\vartheta=&-\frac{\pi(-1)^{m+r}{}_2F_1\left(-\frac{1}{2},m+r+\frac{1}{2};m+r+\frac{3}{2};-1\right)}{2(2m+2r+1)}\\&-\frac{\sqrt{\pi}\Gamma(m+r+\frac{1}{2})\left(\psi(m+r+\frac{1}{2})-\psi(m+r+2)\right)}{8\Gamma(m+r+2)}\\&-i\frac{2(-1)^{m+r}{}_3F_2\left(-\frac{1}{2},m+r+\frac{1}{2},m+r+\frac{1}{2};m+r+\frac{3}{2},m+r+\frac{3}{2};-1\right)}{(2m+2r+1)^2}\end{aligned} \tag{A22}$$

$$\int_0^{\pi/2}e^{i(2m+2r-2n-1)\vartheta}\sqrt{e^{2i\vartheta}-1}d\vartheta=-\frac{\sqrt{\pi}\Gamma(m+r-n-\frac{1}{2})}{4\Gamma(m+r-n+1)}+i\frac{2\sqrt{2}(-1)^{m+r-n-1}{}_2F_1(1,m+r-n+1;m+r-n+\frac{1}{2};-1)}{2m+2r-2n-1}. \tag{A23}$$

and noting that $\ln(kde^{i\vartheta}/2)=i\vartheta+\ln(kd/2)$ and ${}_2F_1\left(-\frac{1}{2},m+r+\frac{1}{2};m+r+\frac{3}{2};-1\right)-2\sqrt{2}{}_2F_1(1,m+r+2;m+r+\frac{3}{2};-1)=0$ yields

$$\begin{aligned}I_{nI}(x)=&\frac{1}{2\pi}\sum_{m=0}^{\infty}\left\{\sum_{r=0}^{\infty}\frac{(-1)^{m+r}\Gamma\left(n+\frac{3}{2}\right)\Gamma(m+r+\frac{1}{2})}{(2m)!r!(n+r+1)!(m+r+1)!}\left(\frac{kd}{2}\right)^{2m+2r+1}\right.\\&\times\left(2\ln\left(\frac{kd}{2}\right)+\psi(m+r+\tfrac{1}{2})-\psi(m+r+2)-\psi(r+1)-\psi(n+r+2)\right)\\&\left.-\sum_{r=0}^{n}\frac{(-1)^m(n-r)!\Gamma\left(n+\frac{3}{2}\right)\Gamma(m+r-n-\frac{1}{2})}{(2m)!r!(m+r-n)!}\left(\frac{kd}{2}\right)^{2m+2r-2n-1}\right\}\left(\frac{2x}{d}\right)^{2m}\end{aligned} \tag{A24}$$

[1]P. J. Walker, "Wide range electrostatic loudspeakers. I, II, and III, " Wireless World, **61**, pp. 208–211, 265–269, 381–384 (1955).
[2]T. F. Hueter and R. H., *Bolt Sonics* (Wiley, New York, 1955), p. 58.
[3]R. D. Ford, "Principles of sound radiation," in *Loudspeaker and Headphone Handbook*, edited by J. N. Borwick (Butterworths, London, 1988), Chap. 1, pp. 9–12;R. D. Ford, "Principles of sound radiation," in *Loudspeaker and Headphone Handbook*, edited by J. N. Borwick (Butterworths-Heinemann, Oxford, 1994), pp. 10–12.
[4]S. P. Lipshitz, T. C. Scott, and B. Salvy, "On the acoustic impedance of baffled strip radiators," J. Audio Eng. Soc. **43**(7/8), 573–580 (1995).
[5]P. M. Morse and P. J. Rubenstein, "The diffraction of waves by ribbons and by slits," Phys. Rev. **54**, 895–898 (1938).
[6]J. Babinet, "Mémoires d'optique météorologique (Memoirs on meteorological optics)," C. R. Acad. Sci. Paris, **4**, 638 (1837).
[7]C. J. Bouwkamp, "Theoretical and numerical treatment of diffraction through a circular aperture," IEEE Transactions of Antennas and Propagation **18**(2), 152–176 (1970). This is a translation of his PhD dissertation originally published in Dutch in 1941.
[8]T. J. Mellow, and L. M. Kärkkäinen, "On the sound field of an oscillating disk in an open and closed circular baffle," J. Acoust. Soc. Am. **118**(3), 1311–1325 (2005).

[9]T. J. Mellow, and L. M. Kärkkäinen, "A dipole loudspeaker with a balanced directivity pattern," J. Acoust. Soc. Am. **128**(5), 2749–2757 (2010).
[10]T. J. Mellow, "On the sound field of a resilient disk in an infinite baffle," J. Acoust. Soc. Am. **120**(1), 90–101 (2006).
[11]T. J. Mellow, "On the sound field of a resilient disk in free space," J. Acoust. Soc. Am. **123**(4), 1880–1891 (2008).
[12]P. M. Morse and K. U. Ingard, *Theoretical Acoustics* (McGraw-Hill, NY, 1968), p. 364.
[13]H. Lamb, "On the propagation of tremors over the surface of an elastic solid," Philos. Trans. R. Soc. London, Ser. A **203**, 1–42 (1904).
[14]A. Sommerfeld, "Über die Ausbreitung der Wellen in der drahtlosen Telegraphie (On the propagation of waves in wireless telegraphy)," Ann. Phys. **4**(28), 665–736 (1909).
[15]M. Greenspan, "Piston radiator: Some extensions of the theory," J. Acoust. Soc. Am. **65**(3), 608–621 (1979).
[16]J. F. Kelly and R. J. McGough, "An annular superposition integral for axisymmetric radiators," J. Acoust. Soc. Am. **121**(2), 759–765 (2006).
[17]E. G. Williams, J. D. Maynard, and E. Skudrzyk, "Sound source reconstructions using a microphone array," J. Acoust. Soc. Am. **68**(1), 340–344 (1980).
[18]E. G. Williams, *Fourier Acoustics: Sound Radiation and Nearfield Acoustical Holography* (Academic, San Diego, 1999), pp. 31–34, 89–91.
[19]H. Stenzel, "Die Akustische Strahlung der Rechteckigen Kolbenmembran (The acoustic radiation of the rectangular piston diaphragm)," Acustica **2**, 263–281 (1952).
[20]G. Bank and J. R. Wright, "Radiation impedance calculations for a rectangular piston," J. Audio Eng. Soc. **38**(5), 350–354 (1990).
[21]E. Skudrzyk, *The Foundations of Acoustics* (Springer-Verlag, New York, 1971), p. 656.
[22]S. Wolfram, *The Mathematica Book*, 5th ed. (Wolfram Media, Champaign, IL, 2003). Symbolic computation by MATHEMATICA.
[23]J. W. S. Rayleigh, *The Theory of Sound* (Dover, NY, 1945), Vol. II, pp.107, 139, and 162.